JACS
JOURNAL OF THE AMERICAN CHEMICAL SOCIETY
Article
pubs.acs.org/JACS

# Electronic and Exchange Coupling in a Cross-Conjugated D−B−A Biradical: Mechanistic Implications for Quantum Interference Effects

Martin L. Kirk,*[,‡] David A. Shultz,*[,†] Daniel E. Stasiw,[†] Diana Habel-Rodriguez,[‡] Benjamin Stein,[‡] and Paul D. Boyle[†,§]

[‡]Department of Chemistry, The University of New Mexico, MSC03 2060, Albuquerque, New Mexico 87131-0001, United States
[†]Department of Chemistry, North Carolina State University, Raleigh, North Carolina 27695-8204, United States

Supporting Information

**ABSTRACT:** A combination of variable-temperature EPR spectroscopy, electronic absorption spectroscopy, and magnetic susceptibility measurements have been performed on $Tp^{Cum,Me}Zn$(SQ-*m*-Ph-NN) (**1-meta**) a donor−bridge−acceptor (D−B−A) biradical that possesses a cross-conjugated *meta*-phenylene (*m*-Ph) bridge and a spin singlet ground state. The experimental results have been interpreted in the context of detailed bonding and excited-state computations in order to understand the excited-state electronic structure of **1-meta**. The results reveal important excited-state contributions to the ground-state singlet−triplet splitting in this cross-conjugated D−B−A biradical that contribute to our understanding of electronic coupling in cross-conjugated molecules and specifically to quantum interference effects. In contrast to the conjugated isomer, which is a D−B−A biradical possessing a *para*-phenylene bridge, admixture of a single low-lying singly excited D → A type configuration into the cross-conjugated D−B−A biradical ground state makes a negligible contribution to the ground-state magnetic exchange interaction. Instead, an excited state formed by a Ph-NN (HOMO) → Ph-NN (LUMO) one-electron promotion configurationally mixes into the ground state of the *m*-Ph bridged D−A biradical. This results in a double (dynamic) spin polarization mechanism as the dominant contributor to ground-state antiferromagnetic exchange coupling between the SQ and NN spins. Thus, the dominant exchange mechanism is one that activates the bridge moiety via the spin polarization of a doubly occupied orbital with phenylene bridge character. This mechanism is important, as it enhances the electronic and magnetic communication in cross-conjugated D−B−A molecules where, in the case of **1-meta**, the magnetic exchange in the active electron approximation is expected to be $J \sim 0$ cm$^{-1}$. We hypothesize that similar superexchange mechanisms are common to all cross-conjugated D−B−A triads. Our results are compared to quantum interference effects on electron transfer/transport when cross-conjugated molecules are employed as the bridge or molecular wire component and suggest a mechanism by which electronic coupling (and therefore electron transfer/transport) can be modulated.

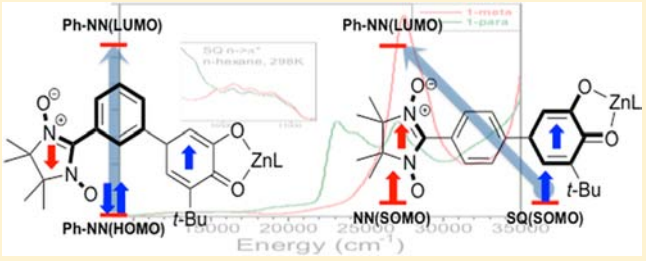


## INTRODUCTION

The relationship between donor−acceptor (D−A) interactions and molecular electronics began when Aviram and Ratner[1] suggested that a donor−bridge−acceptor (D−B−A) molecule could function as a rectifier. The D−A paradigm has also contributed extensively to our understanding of photoinduced electron transfer (PET),[2−8] where a spin exchange interaction ($J$) exists between radical pair electrons in the $D^+$−$A^-$ charge-separated state. Based on the work of Anderson and others,[9−12] Wasielewski and co-workers[4−8,13] have shown that the rate of photoinduced electron transfer is directly proportional to both $J$ and the square of the electronic coupling matrix element, $\mathbf{H}_{ab}$, for a variety of D−B−A triads in the nonadiabatic regime. The magnitude of the electronic coupling in D−A systems typically displays an exponential decay as a function of increasing D−A distance[5] and is modulated by the intrinsic electronic structure of the bridge that connects D and A. A wide array of molecular structure-property relationships have been probed by PET rates in D−B−A excited states,[3,7,14,15] theoretical and computational studies,[15−19] and the magnitude of the magnetic exchange interaction in $D^+$−B−$A^-$ charge-separated states.[4,6,8,13] We have shown that stable D−B−A biradicals are effective ground-state analogues of charge-separated states.[20−22] A key finding for D−B−A biradicals that possess conjugated bridges is the importance of a single D → A charge transfer excited state that configurationally mixes into the ground state to stabilize the spin triplet.[20−22]

In contrast to electron-transfer systems that utilize conjugated bridges and display a well-known reduction in bridge-mediated electronic coupling as a function of distance, the use of cross-conjugated bridges dramatically reduces D−A coupling at parity of D−A distance.[15] The rates of photoinduced charge separation in D−A molecules that possess cross-conjugated bridges are ∼30 times slower than rates of charge separation in D−A molecules having isomeric,

Received: June 2, 2013
Published: August 22, 2013

   dx.doi.org/10.1021/ja405354x | J. Am. Chem. Soc. 2013, 135, 14713−14725

conjugated bridges.[15,23] Since the rate constant varies as $\mathbf{H}_{ab}^2$, this implies that $\mathbf{H}_{ab}$(cross-conjugated) ~ $\mathbf{H}_{ab}$(conjugated)/$(30)^{1/2}$. In related electron transport systems where single molecules bridge nanoelectrode assemblies, the use of cross-conjugated molecules results in an effective barrier to efficient electron transmission.[16−19,24] The reduction in transmission derives from destructive antiresonances (quantum interference effects)[17−19,24−28] that tend to cancel competing pathway contributions to electron transfer/transport,[27,29−34] and it has recently been suggested that fast and reproducible switching[16] can be actuated through the use of these quantum interference effects. Thus, studies of cross-conjugated D−B−A systems represent an important area of research directly related to molecular electronics. In fact, theoretical calculations suggest that the electron density distribution affects transmission properties in cross-conjugated bridges such as *meta*-phenylene (*m*-Ph) in a predictable way,[15−19] effectively moving the destructive interference feature responsible for insulator behavior to positive and negative potentials relative to the Fermi energy and turning on conduction.

We have used a combined spectroscopic and magnetic approach augmented by bonding and excited-state computations to understand the electronic origin of the ground-state magnetic exchange and electronic coupling ($\mathbf{H}_{ab}$) in D−B−A biradicals,[22] where donor = semiquinone (SQ) and acceptor = nitronylnitroxide (NN). This has allowed us to determine $\mathbf{H}_{ab}$ in the adiabatic regime. A valence bond configuration interaction (VBCI) model[11,20,21,35,36] has been used to relate $\mathbf{H}_{ab}$ to the exchange coupling parameter, 2*J*, via eq 1 (where $K_0$ is the exchange splitting of the dominantly contributing charge-transfer (CT) excited state and *U* is the mean CT energy).

$$J_{ab} = \frac{\mathbf{H}_{ab}^2 K_0}{U^2 - K_0^2} \tag{1}$$

Herein, we describe structural, spectroscopic, magnetic, and computational studies of an SQ-(*m*-Ph)-NN biradical bridged by the cross-conjugated *m*-Ph spacer. To the best of our knowledge, this is the first detailed electronic structure study of a D−B−A biradical system directed toward understanding the effects of bridge connectivity on electronic coupling at parity of D and A and the composition of the bridge. In particular, we have determined the excited-state origin of the ground-state exchange in a cross-conjugated D−B−A triad (**1-meta**), which gives rise to quite different electronic and exchange couplings compared to the conjugated *para*-isomer. Our results suggest revealing differences in electronic coupling for D−B−A molecules that possess cross-conjugated bridges compared to their conjugated bridge counterparts. We show that the use of cross-conjugated bridges in D−B−A biradicals: (1) changes the sign of the magnetic exchange interaction from ferromagnetic to antiferromagnetic; (2) dramatically reduces key CT contributions to the ground-state exchange; and (3) allows dynamic spin polarization contributions to the exchange to dominate. Importantly, our findings have implications for molecular design features in electron transfer/transport systems that are subject to quantum interference effects.

## EXPERIMENTAL SECTION

**General Considerations.** Reagents and solvents were purchased from commercial sources and used as received unless otherwise noted. $^1$H and $^{13}$C NMR spectra were recorded on a Varian Mercury 400 MHz or a Varian Mercury 300 MHz spectrometer at room temperature. $^1$H and $^{13}$C chemical shifts are listed in parts per million (ppm) and are referenced to residual protons or carbons of the deuterated solvents, respectively. Infrared spectra were recorded on a Brüker Vertex 80v spectrometer with Brüker Platinum ATR attachment. Elemental analyses were performed by Atlantic Microlabs, Inc. High-resolution mass spectra were obtained at the NCSU Department of Chemistry Mass Spectrometry Facility. Compounds **4**,[37,38] **7**,[39] **10**,[40] and **13**[41] were prepared according to published procedures.

**Electronic Structure Calculations.** Spin unrestricted gas-phase geometry optimizations were performed at the density functional level of theory using the Gaussian 03 software package.[42] All calculations employed the B3LYP hybrid functional. A 6-31G(d′p′) split-valence basis set with polarization functions was used for all atoms. Input files were prepared using the molecule builder function in the Gaussview software package, and the *t*-butyl substituent on the semiquinone was modeled as a methyl group. Frontier molecular orbitals (MOs) were generated for the optimized ground states. Optical excitation energies and oscillator strengths were calculated using time-dependent DFT (TDDFT) methods. These TDDFT calculations were performed on the optimized ground-state geometries, and the first 25 excited states were calculated. Electron density difference maps were constructed utilizing custom in-house software.[43] Complete active space self-consistent field (CASSCF) calculations, which are based on a multiconfigurational approach, were carried out in the ORCA SCF-MO program.[44] The CASSCF calculations employed a def2-TZVP triple-$\zeta$ basis set with added polarization functions and a convergence tolerance for the orbital gradient of $1e^{-4}$. The energy was optimized for the singlet and triplet ground states with respect to the coefficients of the configurations that contribute to each state as well as the MO coefficients of the spin restricted orbitals.

**Electron Paramagnetic Resonance.** EPR spectra were recorded on a JEOL JES-FA100 EPR spectrometer, with low-temperature spectra recorded by use of an ARS-LTR continuous flow cryostat. A 2 mM sample was prepared in freshly distilled 2-methyl-tetrahydrofuran and degassed, and the spectra collected in a J. Young tube. Collected variable-temperature (VT) data were fit using the Curie law and a Boltzmann distribution of $S = 1$ to 0 ground states.

**Magnetic Susceptibility.** Magnetic susceptibility measurements were collected on a Quantum Design MPMS-XL7 SQUID magnetometer with an applied field of 0.7 T. A microcrystalline sample (~20 mg) was loaded into a gelcap/straw sample holder and mounted to the sample rod with Kapton tape for VT measurements. Collected raw data were corrected with a straight line for diamagnetic response of sample container and molecular diamagnetism using Pascal's constants as a first approximation, where the slope of the line represents the residual diamagnetic correction.

**Electronic Absorption Spectroscopy.** Low-temperature electronic absorption spectra were obtained on a Hitachi U-3501 UV−vis-NIR spectrometer capable of scanning a wavelength region between 185 and 3200 nm using a double-beam configuration at 2.0 nm resolution. The instrument was calibrated to the 656.1 nm deuterium line using the corresponding Hitachi software option. Variable-temperature electronic absorption measurements required the removal of the cuvette holder assembly in order to accommodate the cryostat in the sample chamber. A custom designed Janis STVP-100 continuous flow cryostat was mounted in the sample holder allowing for VT electronic absorption data to be conveniently collected in the 5−300 K temperature range. Sample temperature was monitored with a Lakeshore silicon diode (PT-470) and regulated by a combination of helium flow and dual heater assemblies. Solid-solution spectra were collected on thin polystyrene (MW = 280 000) polymer films prepared by evaporation of saturated polystyrene solutions cast on glass plates.

**Synthesis.** *3′-(tert-Butyl)-4′-hydroxy-[1,1′-biphenyl]-3-carboxaldehyde (**6**).* To a 50 mL Schlenk flask, 1.00 g (4.36 mmol) 4-bromo-2-*tert*-butylphenol, **4**, was added with 782 mg (5.23 mmol) (3-formylphenyl)boronic acid, **5**, and 273 mg (0.24 mmol) tetrakis-(triphenylphosphine) palladium(0), with ~15 mL tetrahydrofuran under nitrogen atmosphere. A 2 M solution of potassium carbonate was degassed, and 7.6 mL was added to the reaction flask via syringe.

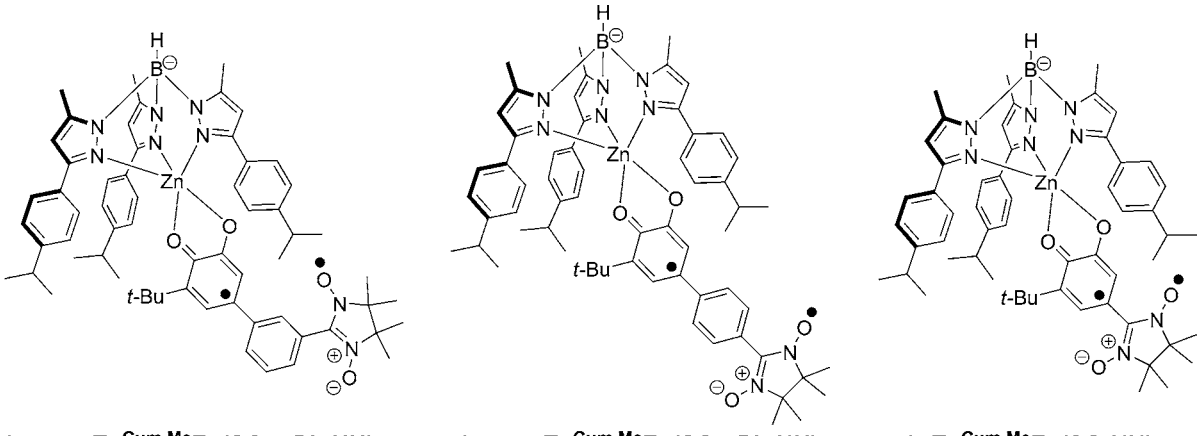


**Figure 1.** Bond line drawings for compounds discussed in this study.

The reaction was refluxed 16 h and checked by thin layer chromatography (TLC) (75% ethyl acetate in hexanes) to ensure product formation. The reaction was cooled to room temperature and quenched by addition of ∼10 mL deionized water with stirring in air for 30 min. The reaction mixture was transferred to a separatory funnel, washed with saturated sodium bicarbonate, and then extracted with dichloromethane. The dichloromethane extractions were dried over sodium sulfate, and the solvent was removed under reduced pressure. The resulting brown oil was dissolved in diethyl ether, and approximately an equal volume of petroleum ether was added then filtered through medium porosity sintered glass. The solvent was removed under reduced pressure yielding a yellow solid which was recrystallized from warm ethyl acetate to yield 721 mg of compound **6** (65% yield). $^1$H NMR (DMSO-$d_6$, $\delta$): 10.07 (s, 1H), 9.64 (s, 1H), 8.08 (t, $^4J$ 1.6 Hz, 1H), 7.91 (dt, $^3J$ 7.7 Hz, $^4J$ 1.6 Hz, 1H), 7.79 (dt, $^3J$ 7.7 Hz, $^4J$ 1.6 Hz, 1H), 7.62 (t, $^3J$ 7.7 Hz, 1H), 7.46 (d, $^3J$ 2.2 Hz, 1H), 7.39 (dd, $^3J$ 8.2 Hz, $^3J$ 2.2 Hz, 1H), 6.91 (d, $^3J$ 8.2, 1H), 1.41 (s, 9H). $^{13}$C NMR (DMSO-$d_6$, ppm): 193.97, 156.88, 142.42, 137.40, 136.45, 132.66, 130.25, 129.95, 127.98, 127.40, 125.95, 125.61, 117.43, 35.05, 29.92. IR (cm$^{-1}$): 3310 (br, $\nu$O−H), 1690 (s, $\nu$C═O). Elemental analysis: calcd (C: 80.28, H: 7.13), found: (C: 79.99, H: 7.09).

*5′-(tert-Butyl)-3′,4′-dioxo-3′,4′-dihydro-[1,1′-biphenyl]-3-carboxaldehyde (**8**).* To a 50 mL pear shaped flask, 593 mg (2.33 mmol) **6** and 1.33 g (4.75 mmol) 7 were added with 2 mL dimethylformamide and stirred shielded from light for 30 h. After about 30 min, the solution changed color from light yellow to dark green. Reaction progress is monitored by TLC (50% ethyl acetate in hexanes) and $^1$H NMR. Once all of **6** had been consumed, the reaction was poured into 100 mL water, transferred to a separatory funnel, and extracted with ethyl acetate. The organic phase was washed three times with saturated sodium bicarbonate solution and then twice with half-saturated sodium chloride solution. The organic phase was then collected and dried over sodium sulfate, and the solvent removed under reduced pressure to yield 460.7 mg of compound **8** (70% yield). $^1$H NMR ($CDCl_3$, $\delta$): 8.05 (s, 1H), 7.95 (d, $^3J$ 7.9 Hz, 1H), 7.83 (d, $^3J$ 7.9 Hz, 1H), 7.64 (t, $^3J$ 7.9 Hz, 1H), 7.16 (d, $^3J$ 2.0 Hz, 1H), 6.49 (d, $^3J$ 2.0 Hz, 1H), 1.24 (s, 9H). $^{13}$C NMR ($CDCl_3$, ppm): 191.31, 180.14, 179.26, 151.59, 150.36, 137.98, 136.86, 134.05, 132.07, 131.95, 130.01, 127.10, 124.33, 35.71, 29.08. IR (cm$^{-1}$): 1702 (s, $\nu$C═O), 1653 (s, $\nu$C═O). Elemental analysis: calcd (C: 71.82, H: 5.67), found (C: 72.01, H: 5.67).

*3′-(tert-Butyl)-4′,5′-dihydroxy-[1,1′-biphenyl]-3-carboxaldehyde (**9**).* The quinone, **8**, was dissolved in 10 mL tetrahydrofuran and transferred to a separatory funnel. To a 25 mL Erlenmeyer flask, 328 mg (1.86 mmol) ascorbic acid was added and dissolved in 10 mL deionized water. The ascorbic acid was added to the separatory funnel containing **8** and shaken. The green color of **8** instantly changed to light yellow. Saturated sodium chloride solution was added, and the product was extracted by ethyl acetate. The organic phase was dried over sodium sulfate, and the solvent removed under reduced pressure. The product is purified by flash chromatography (20% ethyl acetate in hexanes) to yield 401 mg of compound **9** (86% yield). $^1$H NMR (DMSO-$d_6$, $\delta$): 10.08 (s, 1H), 9.64 (s, 1H), 8.33 (s, 1H), 8.02 (s, 1H), 7.83 (m, 2H), 7.64 (t, $^3J$ 7.7 Hz, 1H), 7.02 (s, 1H), 6.97 (s, 1H), 1.40 (s, 9H). $^{13}$C NMR (DMSO-$d_6$, ppm): 193.47, 145.61, 144.48, 142.00, 136.76, 136.17, 132.02, 129.71, 128.78, 127.121, 126.99, 115.71, 111.33, 34.51, 29.41. IR (cm$^{-1}$): 3140 (br, $\nu$O−H), 1678 (s, $\nu$C═O). Mass spectrometry ($m/z$): (M + H)$^+$ calcd for $C_{17}H_{18}O_3$: 271.1334; found: 271.1327.

*2-(3′-(tert-Butyl)-4′,5′-dihydroxy-[1,1′-biphenyl]-3-yl)-4,4,5,5-tetramethylimidazolidine-1,3-diol (**11**).* To a 10 mL pear-shaped flask, 331 mg (1.22 mmol) **9** and 279 mg (1.88 mmol) *N,N′*-(2,3-dimethylbutane-2,3-diyl)bis(hydroxylamine), **10**, were added with a magnetic stir bar. A Schlenk adapter was attached and sealed with a thick septum. The system was then attached to a Schlenk line and pump/purged with nitrogen 5 times. In a 50 mL Schlenk flask 15 mL methanol was degassed, and 2 mL was added to the reaction flask. The reaction mixture was stirred for 24 h at room temperature. The resulting opaque white solution was vacuum filtered to collect a white solid that was collected into a sample vial and dried under reduced pressure yielding 339 mg of compound **11** (80% yield). $^1$H NMR (DMSO-$d_6$, $\delta$): 9.52 (br s, 1H), 8.14 (br s, 1H), 7.77 (s, 2H), 7.62 (s, 1H), 7.35 (m, 2H), 6.95 (s, 1H), 6.89 (s, 1H), 4.53 (s, 1H), 1.38 (s, 9H), 1.08 (d, $^3J$ 4.4 Hz, 12H). $^{13}$C NMR (DMSO-$d_6$, ppm): 145.22, 143.55, 142.22, 140.47, 135.78, 130.56, 127.77, 126.40, 126.32, 124.81, 90.32, 66.03, 34.29, 29.35, 24.25, 17.06.

*3-tert-Butyl-4-(phenyl-3-nitronylnitroxide)-o-catechol (**12**).* To a 100 mL round-bottom flask, 49 mg (0.12 mmol) **11** was added with 20 mL diethyl ether, 10 mL fresh pH 7 buffer, and magnetically stirred at 0 °C. To a 60 mL separatory funnel, 47 mg (0.18 mmol) $I_2$ was added with 30 mL diethyl ether and shaken. The solution of $I_2$ was added dropwise with stirring to the reaction mixture. After all of the iodine was added, the reaction stirred for 15 min, and then 100 mL pH 7 buffer was added. The reaction was transferred to a separatory funnel and washed with 50 mL saturated thiosulfate solution twice followed by 50 mL saturated sodium chloride solution. The organic phase was collected and dried over magnesium sulfate, and the solvent removed under reduced pressure to yield 53 mg of **12** (>99% yield). IR (cm$^{-1}$): 3300 (br, $\nu$O−H). EPR (X-band, 298 K): pentet (1:2:3:2:1), $a_N$ = 7.6 G. Mass spectrometry ($m/z$): (M + H − O)$^+$ calcd for $C_{23}H_{31}N_2O_3$: 383.2335; found: 383.2322.

*Tp$^{Cum,Me}$Zn(SQ-m-Ph-NN) (**1-meta**).* To a 25 mL oven-dried Schlenk flask, 42 mg (0.11 mmol) **12** and 69 mg (0.10 mmol) **13** were added with a stir bar. The reaction vessel was pump/purged with nitrogen, and about 5 mL methanol distilled over calcium hydride was added via purged syringe. The reaction was stirred under inert atmosphere for 2 h. Afterward, the reaction was opened to air, stirred overnight, and then filtered through slow filter paper. The filter paper containing the product was placed in a beaker, and the olive green solid was dissolved in dichloromethane. The new solution was filtered


dx.doi.org/10.1021/ja405354x | J. Am. Chem. Soc. 2013, 135, 14713−14725

**Scheme 1**

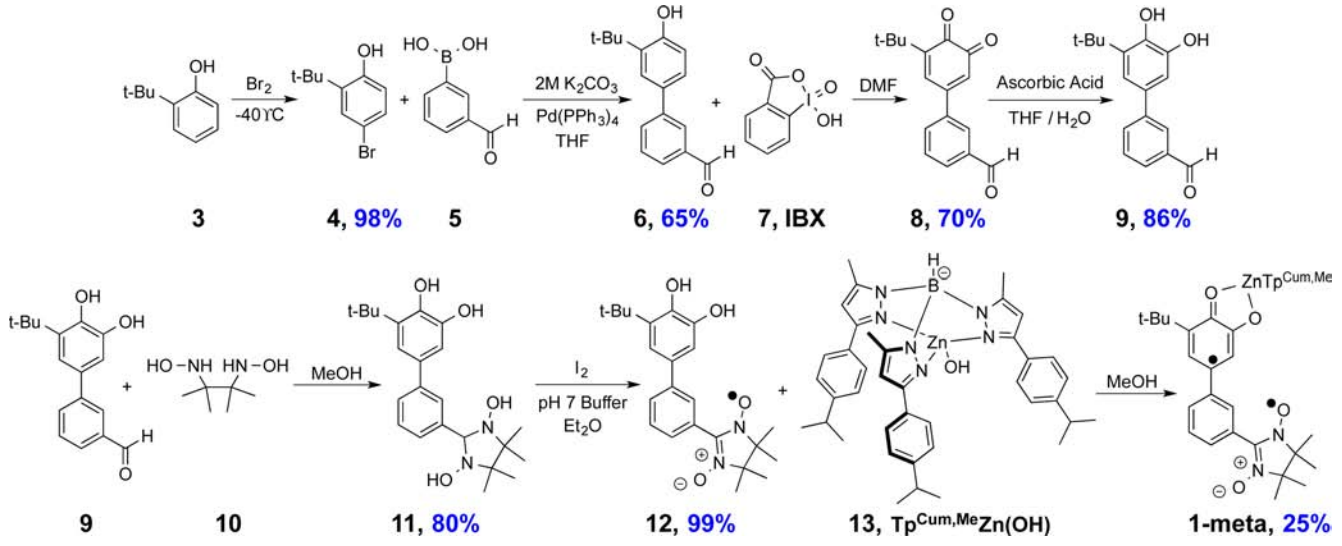


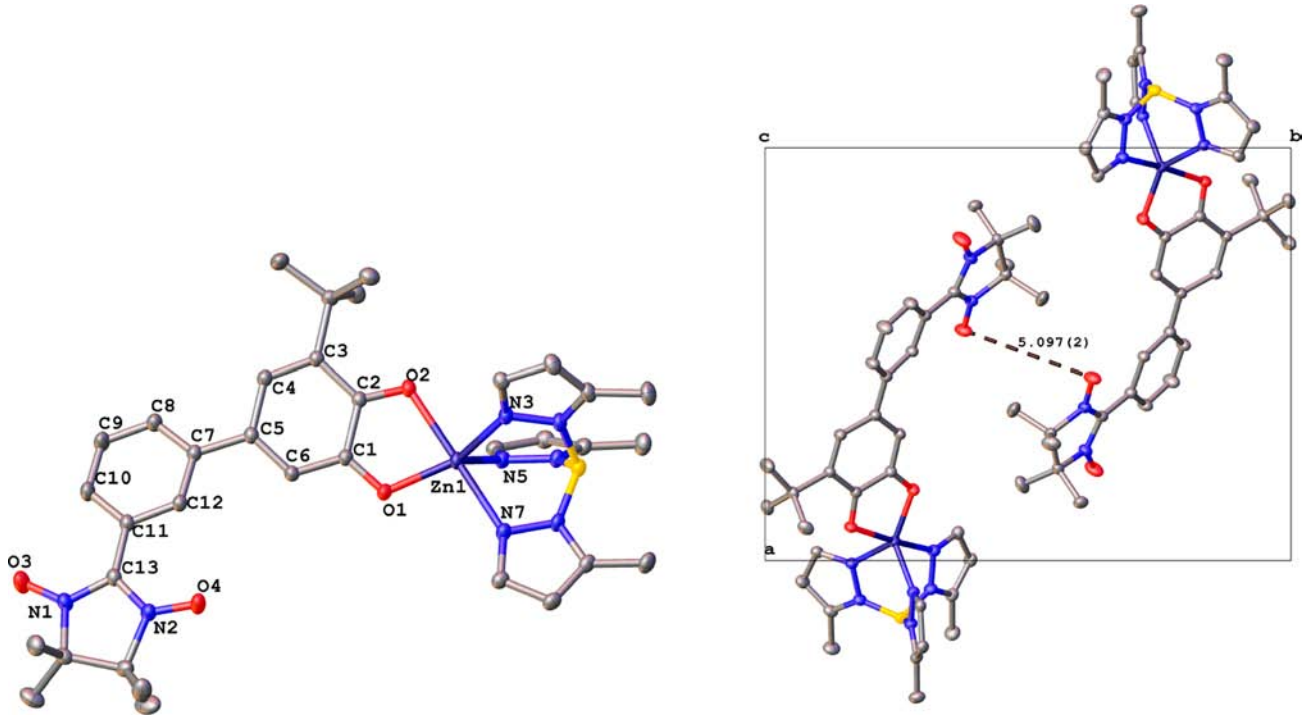


**Figure 2.** (Left) Thermal ellipsoid plot of **1-meta** with H and cumenyl groups removed for clarity. (Right) Crystal packing of **1-meta** along the 001 axis showing the closest oxygen–oxygen contact for the NN intermolecular interaction.

again to remove any salts and yielded 27 mg of **1-meta** (25% yield). The product was crystallized by slow evaporation of n-hexane and a few drops of dichloromethane. Mass spectrometry ($m/z$): $(M + H)^+$ calcd for $C_{62}H_{73}BN_8O_4Zn$: 1068.5139; found: 1068.5226.

## RESULTS AND DISCUSSION

**Synthesis of Biradical Complex 1-meta.** The compounds in this study (**1-meta**, **1-para**, and **2**) are shown in Figure 1. The synthesis and characterization of **1-para** and the parent complex, **2**, have been presented in an earlier work,[45,46] whereas **1-meta** has been synthesized by a newly developed route, outlined in Scheme 1, which requires no protecting groups.

Commercially available phenol **3** was brominated at low temperature to yield phenol **4** in excellent yield and then subjected to Suzuki coupling with boronic acid **5** to yield biarylphenol **6**. Oxidation of **6** to quinone **8** was achieved with IBX (**7**).[39] Reduction of quinone **8** to catechol **9** as a solution in tetrahydrofuran was easily carried out in a separatory funnel by shaking with an aqueous solution of ascorbic acid. Compound **9** was condensed with bishydroxylamine **10** followed by oxidation to yield catechol nitronylnitroxide **12** in excellent yield. Semiquinone complex formation yielding **1-meta** was affected using compounds **12** and **13** following standard procedures.[47,48] Crystals of **1-meta** were grown by slow evaporation of an n-hexane solution containing a few drops of dichloromethane to dissolve **1-meta**.


dx.doi.org/10.1021/ja405354x | J. Am. Chem. Soc. 2013, 135, 14713–14725

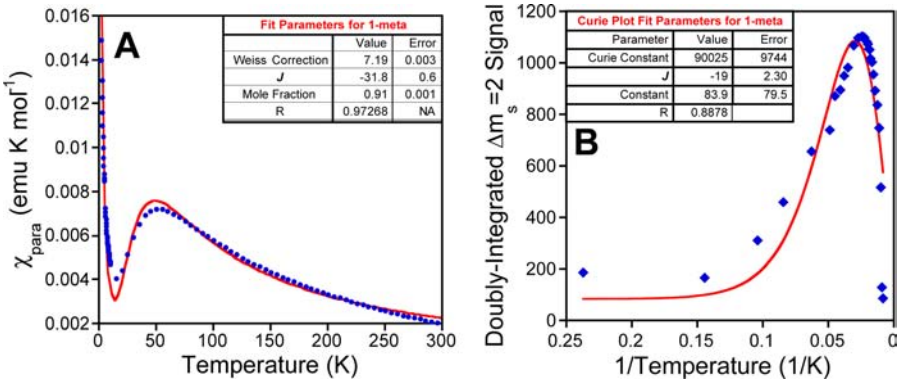


**Figure 3.** (A) Magnetic susceptibility of **1-meta** from 2 to 300 K with constant field of 7000 Oe. Inset: Fit parameters and corresponding errors. (B) VT-EPR Curie plot. Doubly integrated $\Delta m_S = 2$ biradical signal was used to monitor triplet concentration as a function of temperature.

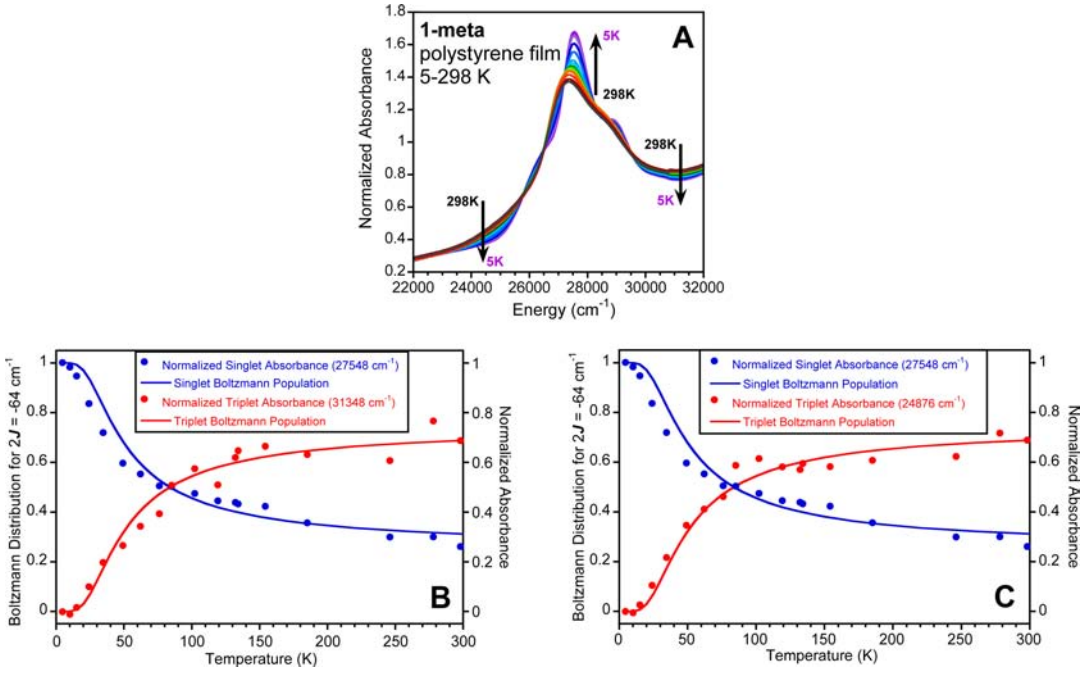


**Figure 4.** (A) Expanded view of the VT electronic absorption spectra for **1-meta**. Full spectral plot is available in the Supporting Information (SI). (B,C) Calculated Boltzmann distributions for singlet and triplet populations based on the magnetic exchange coupling determined by magnetic susceptibility measurements. The individual data points represent normalized absorbance values at a given energy as a function of temperature.

**X-ray Crystal Structure of 1-meta.** The thermal ellipsoid plot of **1-meta** is shown in Figure 2 (left). Crystallographic details and important bond lengths and torsion angles are given in Tables S1 and S2, respectively. The *o*-SQ bond lengths fit within typical values with a negligible structural deviation parameter[46] of $\Sigma|\Delta_i| = 0.02$ Å (however, $\Sigma|\Delta_i| = 0.02$ Å for **1-para**, but $\Sigma|\Delta_i| = 0.19$ Å for **2**) consistent with, but not proof of, the lack of SQ(donor)−NN(acceptor) interaction dictated by the cross-conjugated *m*-Ph bridge. NN bond lengths are also within typical values with a negligible structural deviation parameter of $\Sigma|\Delta_i| = 0.02$ Å based on the previously reported Catechol−NN structure.[46]

**SQ−NN Exchange Coupling in 1-meta Measured by Magnetic Susceptibility, Variable-Temperature Electronic Absorption and EPR Spectroscopy.** The magnetic susceptibility data for **1-meta** are plotted in Figure 3A as $\chi_{para}$ vs T. It is clear that by the shape of the curve outlined by the data that the complex is an antiferromagnetically coupled "spin-dimer" with a minor paramagnetic impurity. To analyze these magnetometry data, we use the Heisenberg−Dirac−van Vleck Hamiltonian given in eq 2 where $S_1 = S_2$ represent the spin operators for two different $S = 1/2$ spin containing groups (SQ and NN) on the same ligand.[46]

$$\hat{H} = -2J\hat{S}_i \cdot \hat{S}_j \tag{2}$$

As shown in Figure 3A, the data were fit using eq 3 where $\chi_{para}$ is the molar magnetic susceptibility, $\theta$ is a Curie−Weiss correction term, $c$ is the mole fraction of pure **1-meta**, and $J$ is the exchange coupling for **1-meta.** The second term in eq 3 accounts for $S = 1/2$ paramagnetic impurity. Nonlinear least-squares fitting gave $J_{SQ-NN} = -32$ cm$^{-1}$: net antiferromagnetic coupling of constituent SQ and NN radicals through the *m*-Ph bridge.

$$\chi_{para} = \left(\frac{Ng^2\mu_B^2}{3k_B(T-\theta)}\frac{6e^{2J/k_BT}}{1+3e^{2J/k_BT}}\right)c + \left(\frac{0.375}{T}\right)(1-c) \tag{3}$$


dx.doi.org/10.1021/ja405354x | J. Am. Chem. Soc. 2013, 135, 14713−14725

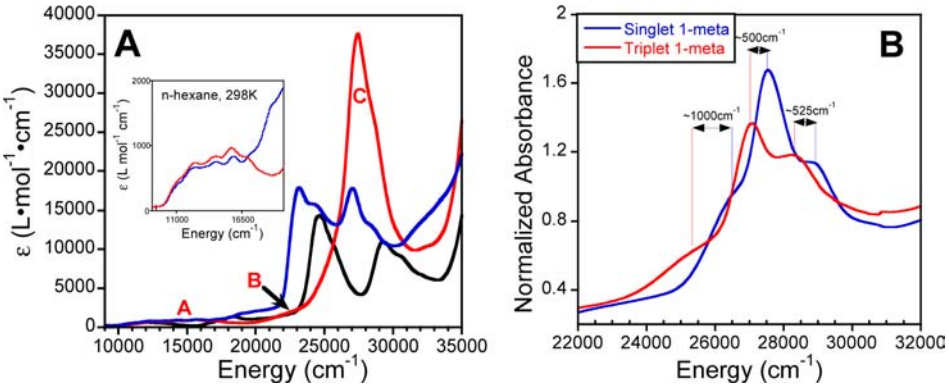


**Figure 5.** (A) Overlay of electronic absorption spectra for **1-meta** (red), **1-para** (blue), and **2** (black). (B) Pure singlet (blue) and pure triplet (red) spectra for **1-meta**. Note that transitions for triplet **1-meta** are shifted ∼500−1000 $cm^{-1}$ to lower energy compared to singlet **1-meta**.

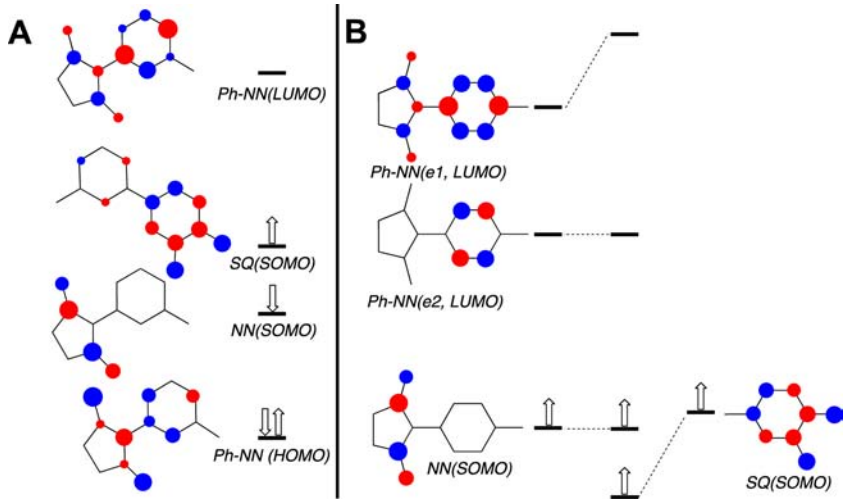


**Figure 6.** (A) Important frontier $\pi$-orbitals for **1-meta**. (B) SQ-Ph-NN(LUMO) interactions in **1-para**. The SQ(SOMO) → Ph-NN(e1, LUMO) CT is responsible for the ferromagnetic exchange interaction in the VBCI model. Note that in **1-para**, the SQ(SOMO) → Ph(e2, LUMO) transition is orbitally forbidden, while in **1-meta** it is allowed and contributes to band C, see text.

The closest oxygen−oxygen intermolecular distance in the **1-meta** unit cell, Figure 2 (right), is 5.1 Å which is greater than the distance observed for dominant intermolecular contributions to exchange coupling for nitronylnitroxides.[49−51] Even though intermolecular interactions at this distance are expected to be weak, solution phase (∼2 mM **1-meta**) variable-temperature EPR (VT-EPR) spectra were collected to confirm the exchange coupling determined by magnetometry. The VT-EPR Curie plot displayed in Figure 3B made use of the doubly integrated, formally forbidden $\Delta m_S = 2$ transition to determine triplet concentration as a function of temperature. The EPR Curie plot was fit by a combination of the Curie Law and a Boltzmann distribution as shown in eq 4 where $C$ is the Curie constant, $k$ is a constant that corrects for poor signal-to-noise ratio, and $J$ is the magnetic exchange coupling ($J \approx -19$ $cm^{-1}$) which is just over half the value determined by magnetometry ($J \approx -32$ $cm^{-1}$). However, the fit "misses" the maximum in the doubly-integrated $\Delta m_s = 2$ signal which gives $J \approx 0.8\ kT_{max} = -23$ $cm^{-1}$)

$$I_{EPR} = \frac{C}{T}\frac{3e^{2J/k_BT}}{(1 + 3e^{2J/k_BT})} + k \quad (4)$$

To further relate solution phase measurement of exchange coupling with the magnetic susceptibility results, we correlated the temperature-dependent changes in the electronic absorption spectrum with the Boltzmann populations of the $S = 0$ and 1 ground-state spin levels derived from the magnetic susceptibility determined $J$ value. Variable-temperature electronic absorption spectra were collected on thin polystyrene films of **1-meta** and are displayed in Figure 4A as a stack plot.

The data in Figure 4 clearly show that as the temperature is decreased, the thermally accessible triplet state is depopulated and the ground-state singlet population is increased. Relative changes in the measured absorbance at specific energies are displayed in Figure 4B,C, and their functional form correlates extremely well with the solid lines calculated for Boltzmann populations of the singlet and triplet using $2J = -64$ $cm^{-1}$ from the best fit of eq 4 to the magnetic susceptibility data. Thus, magnetic susceptibility data and VT electronic absorption spectroscopy show that the exchange coupling between the cross-conjugated SQ(donor) and NN(acceptor) radicals is antiferromagnetic ($J \approx -35$ $cm^{-1}$), while VT-EPR spectroscopy suggests a slightly weaker antiferromagnetic coupling. The electronic origin of the magnitude, the sign of the exchange coupling, and the nature of electronic coupling in **1-meta** are discussed below.

**Electronic Absorption Spectroscopy.** Electronic absorption spectroscopy reveals noteworthy differences in the spectra of **1-meta** and **1-para** (Figure 5A). We previously reported a


dx.doi.org/10.1021/ja405354x | J. Am. Chem. Soc. 2013, 135, 14713−14725

**Table 1. Electronic Absorption Spectral Band Assignments for 1-meta**

| band | experimental energy ($cm^{-1}$) | transition | calculated energy ($cm^{-1}$) | calculated oscillator strength | dominant MO contributions to transition[a] |
|---|---|---|---|---|---|
| A | 15 700 | 1 | 13 400 | 0.0102 | SQ-Ph (HOMO) → SQ (SOMO) |
| | | 2 | 18 250 | 0.0034 | NN(SOMO) → Ph-NN(LUMO) - Ph-NN(HOMO) → NN(SOMO) |
| B | 23 000 | 3 | 22 800 | 0.0397 | Ph-NN(HOMO) →SQ(SOMO) + Ph (HOMO)→SQ(SOMO); [Ph-NN(HOMO) → Ph-NN(LUMO)] |
| C | 24 000−29 000 | 4 | 23 950 | 0.0682 | SQ(SOMO) → Ph-NN(e1,LUMO) |
| | | 4′ | 26 450 | 0.0554 | Ph-NN(HOMO) → Ph-NN(LUMO) |
| | | 5 | 28 050 | 0.0691 | NN(SOMO) → Ph-NN(LUMO) + Ph-NN(HOMO) → NN(SOMO) |
| | | 6 | 28 700 | 0.1933 | SQ(SOMO) → SQ-Ph(e2,LUMO) |

[a]See Figure 6A for pertinent **1-meta** frontier orbitals. One-electron promotion contributions given in brackets represent minor contributions to the transition but are important for spin polarization contributions to the magnetic exchange interaction.

detailed electronic structure study of the parent complex, $Tp^{Cum,Me}Zn$(SQ-NN) (**2**), which lacks a bridge between the SQ donor and the NN acceptor and assigned the structured band at ∼25 000 $cm^{-1}$ as a D−A intraligand SQ(SOMO) → NN-(LUMO) charge transfer (ILCT) transition.[20] A subsequent study of **1-para** showed a structured band at ∼23 500 $cm^{-1}$ that was assigned as the D−A intraligand SQ(SOMO) → NN(LUMO) charge transfer (ILCT) transition but with considerable Ph-NN character present in the acceptor orbital (see Figure 6A,B).[21] Indeed, observation of ILCT bands in this energy region is characteristic of $Tp^{Cum,Me}Zn$(SQ−bridge−NN) compounds, and we have used a valence bond configuration interaction model to show that the D−A ILCT band in both **1-para** and **2** are responsible for the extraordinarily large and ferromagnetic biradical exchange coupling (**2**; $J \approx +550$ $cm^{-1}$, **1-para**; $J = +100$ $cm^{-1}$). Obviously, there exist fundamental differences in the underpinning electronic structures of **1-meta** and **1-para** as they relate to the cross-conjugated nature of the bridge fragment in **1-meta**, and this is reflected in their different electronic absorption spectra. Most importantly, the ∼23 500 $cm^{-1}$ SQ(SOMO) → Ph-NN(e1, LUMO) ILCT band characteristic of both **1-para** and **2** appears to be either absent or greatly reduced in intensity in **1-meta**.

The oscillator strength reduction for the SQ(SOMO) → Ph-NN(LUMO) ILCT band is a direct result of the dramatic reduction in orbital overlap between the SQ(SOMO) donor and the Ph-NN(LUMO) acceptor orbitals in **1-meta** compared to **1-para** (Figure 6), indicative of SQ−NN decoupling in **1-meta** due to the cross-conjugated nature of the *m*-Ph bridge. This is a very important distinction since strong configurational mixing of the SQ(SOMO) → bridge−NN(LUMO) ILCT excited configuration ($^3$EC(1), vide infra) into the ground-state configuration (GC) is the dominant mechanism for ferromagnetic biradical exchange in D−B−A biradicals that possess conjugated bridges.[21,22,52] Thus, the lack of a strong SQ-(SOMO) → bridge−NN(LUMO) ILCT band in **1-meta** is a direct probe of the dramatic reduction in D → A coupling that results in a radical shift in both the magnitude and the sign of the exchange: $J = +100$ $cm^{-1}$ in **1-para** and $J = -35$ $cm^{-1}$ in **1-meta** (vida supra).

As shown in Figure 4A, the VT electronic absorption spectra for **1-meta** display a strong temperature dependence with tight isosbestic points, indicating only two species contribute to the VT spectra. The VT electronic absorption data display a marked increase in absorption intensity as a function of increasing temperature at ∼24 800 $cm^{-1}$ with a corresponding decrease in the ∼27 500 $cm^{-1}$ band. In Figure 4B,C we showed that the temperature dependence of the spectra directly correlates with the singlet−triplet gap ($2J = -64$ $cm^{-1}$) determined from solid-state magnetic susceptibility studies (Figure 3A), providing compelling evidence that the average solution conformation is very similar to that observed in the X-ray structure.[45] Since the VT electronic absorption data are comprised of both $^1$GS → $^1$ES and $^3$GS → $^3$ES contributions (GS, ground state; ES, excited state), and the Boltzmann populations of the $^1$GS and $^3$GS are known for a given temperature from the magnitude of the antiferromagnetic exchange, we can use the VT data to construct the pure singlet and pure triplet electronic absorption spectra for **1-meta** (Figure 5B). The similarity of the $^1$GS → $^1$ES and $^3$GS → $^3$ES component spectra indicates that there is no gross change in the GS and ES orbital character as a function of spin and that the observed transitions between ∼24 000 and 32 000 $cm^{-1}$ occur at lower energy for the triplet configuration than for the singlet configuration. For the intense $^1$GS → $^1$ES and $^3$GS → $^3$ES transitions in the ∼27 500 $cm^{-1}$ region, the oscillator strength of the $^1$GS → $^1$ES transition is greater than that of the $^3$GS → $^3$ES transition, and the $^3$ES is stabilized by ∼500 $cm^{-1}$ relative to the singlet state (see Figure 5B).

**Band Assignments.** Electronic absorption spectral band assignments for **1-meta** have been made using a combination of bonding and TDDFT calculations on **1-meta** and Ph-NN,[53] comparisons with our prior spectroscopic studies on $Tp^{Cum,Me}Zn$(SQ), Ph-NN, **1-para**, and **$Tp^{Cum,Me}$Zn(SQ-NN)** (**2**),[20,21] and complete active space multiconfiguration SCF (MC-SCF) calculations. The MC-SCF calculations combine an SCF and a full configuration interaction calculation using a complete active space. The features of the spectrum labeled A−C (Figure 5A) are discussed below, and the one-electron orbital contributions to the transitions are listed in Table 1.

*Band A.* A broad, low-energy transition is observed in the 10 000−17 000 $cm^{-1}$ region ($\varepsilon \sim 625$ $M^{-1}$ $cm^{-1}$) of the electronic absorption spectrum for $Tp^{Cum,Me}Zn$(SQ), and a vibronically structured band has been observed at higher energy (12 000−20 000 $cm^{-1}$) for Ph-NN.[20,53] Weak bands assignable as SQ- and NN-based transitions are also observed in the 10 000−20 000 $cm^{-1}$ region for **1-meta**, **1-para**, and **$Tp^{Cum,Me}$Zn(SQ-NN)** (**2**).[20,21] These data combined with the computationally derived transition energies and oscillator strengths allow us to assign the lower energy component of the broad (10 000−20 000 $cm^{-1}$) structured band (in n-hexane) in **1-meta** as arising from an SQ(HOMO) → SQ(SOMO) transition and the higher energy component as a [NN(SOMO) → Ph-NN(LUMO)− Ph-NN(HOMO) → NN(SOMO)] transition. The SQ-(HOMO) → SQ(SOMO) transition is *y*-polarized, and this polarization direction is orthogonal to the long *z*-axis ($C_2$ axis) of the semiquinone unit and is thus predicted to possess a low


dx.doi.org/10.1021/ja405354x | J. Am. Chem. Soc. 2013, 135, 14713−14725

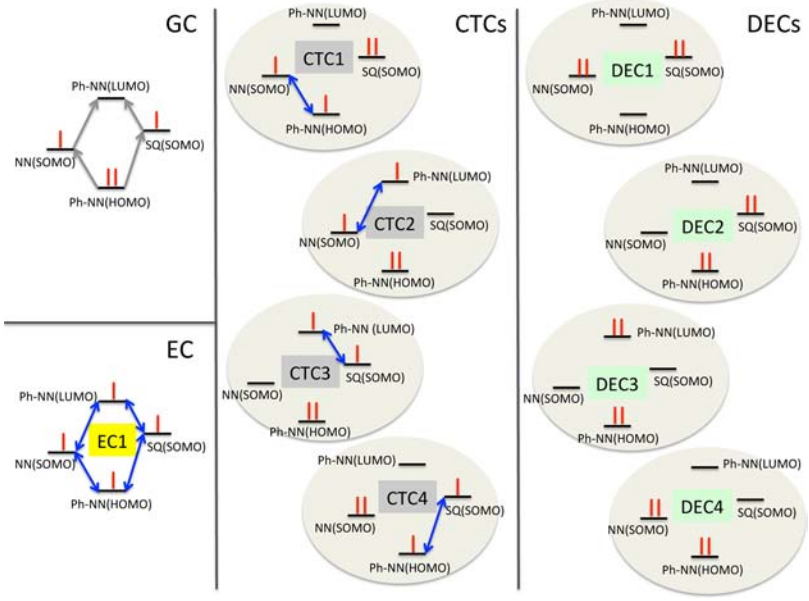


**Figure 7.** Left: The GC and EC of **1-meta**. Double-headed arrows indicate dominant exchange interaction. Middle: Singlet and triplet CTCs that result from one-electron promotions relative to the GC. Right: Closed-shell configurations that derive from one-electron promotions relative to the EC and CTCs. These double excitations relative to the GC produce only singlet DECs. Note that DEC2 and DEC4 can also result from direct SQ(SOMO) → NN(SOMO) and NN(SOMO) → SQ(SOMO) kinetic exchange contributions. Since the <SQ(SOMO)|NN(LUMO)> overlap integral is essentially zero, the kinetic exchange term is also expected to be zero for **1-meta**.

oscillator strength. The [NN(SOMO) → Ph-NN(LUMO)− Ph-NN(HOMO) → NN(SOMO)] transition is also predicted to be weak due to the opposing nature (−) of the transition dipoles for the two one-electron promotions that contribute to the transition. The overall structure and intensity for band A in **1-meta** is virtually identical to the lowest energy band in **1-para**, indicating that transitions 1 and 2 are essentially independent of the bridge connectivity and do not possess appreciable CT character.

*Band B.* Computations indicate that a moderately intense Ph-NN(HOMO) → SQ(SOMO) + Ph (HOMO) → SQ-(SOMO) transition possessing Ph-NN ($\pi$) → SQ ($\pi$) CT character should be anticipated in this energy region. As mentioned above, an intense SQ(SOMO) → Ph-NN(e1, LUMO) transition is observed in this energy region for **1-para** that has been assigned as the dominant contributor to the observed GS ferromagnetic exchange coupling in this molecule. Interestingly, the direction of the Ph-NN ($\pi$) → SQ ($\pi$) CT character (A → D) in transition 3 is the opposite of the SQ ($\pi$) → Ph-NN ($\pi$) CT character (D → A) found in this energy region for **1-para**. The markedly reduced intensity of this band, coupled with no computed SQ(SOMO) → Ph-NN(e1, LUMO) CT contribution, nicely explains the dramatic reduction in ferromagnetic contributions to the ground-state magnetic exchange parameter, allowing weaker antiferromagnetic exchange interactions to dominate.

*Band C.* Band C is the most intense band in the spectrum of **1-meta**, and a number of transitions are computed to contribute to the intensity of this band. A slight shoulder is observed on the low-energy side of band C in the room temperature absorption spectrum at ∼25 000 $cm^{-1}$ that is clearly revealed at 25 000 $cm^{-1}$ in the triplet absorption spectrum (red line, Figure 5B) and at 26 000 $cm^{-1}$ in the singlet absorption spectrum (blue line, Figure 5B). We assign these bands in **1-meta** as arising from exchange split singlet and triplet components of transition 4, which is comprised of SQ(SOMO) → Ph-NN(e1, LUMO) and Ph-NN(HOMO) → Ph-NN(LUMO) one-electron promotions. The SQ ($\pi$) → Ph-NN ($\pi$) CT character present in transition 4 is identical to that observed for **1-para**. However, there are numerous one electron promotion contributions to transition 4 that result in a large reduction in the overall SQ ($\pi$) → Ph-NN ($\pi$) CT character of this transition, yielding reduced CT contributions to ferromagnetic exchange in **1-meta**.

The Ph-NN(HOMO) → Ph-NN(LUMO) one-electron promotion contribution to transition 4 lacks CT character and is computed at lower energy than the Ph-NN(SOMO) → Ph-NN(LUMO) + Ph-NN(HOMO) → Ph-NN(SOMO) transition. This likely reflects the large reduction in electron−electron repulsion that derives from an EC having all of the NN frontier orbitals being singly occupied. TDDFT calculations on Ph-NN show the Ph-NN(HOMO) → Ph-NN(LUMO) transition occurring at 25 959 $cm^{-1}$, and this provides additional support for these one-electron promotions contributing to transition 4. The state that arises from a Ph-NN(HOMO) → Ph-NN(LUMO) (Figure 6A) one-electron promotion is of interest, since this state is known to strongly CI mix into the ground-state wave function to produce negative spin density on the NN bridgehead carbon.[52,54] This configurational mixing is important since the NN(SOMO) wave function is nodal at the bridgehead carbon, and as such, its one-electron occupancy does not directly contribute to the observed spin density at this carbon. This is noteworthy, because we will invoke the role of the Ph-NN(HOMO) → Ph-NN(LUMO) excited state in our discussion of the electronic origin of the observed antiferromagnetic exchange in **1-meta**, vide infra.

Two additional transitions contribute to the intensity of band C. The first is calculated to possess moderate intensity and is assigned as the [NN(SOMO) → Ph-NN(LUMO) + Ph-NN(HOMO) → NN(SOMO)] transition with enhanced intensity due to the additive nature of the two transition


dx.doi.org/10.1021/ja405354x | J. Am. Chem. Soc. 2013, 135, 14713−14725

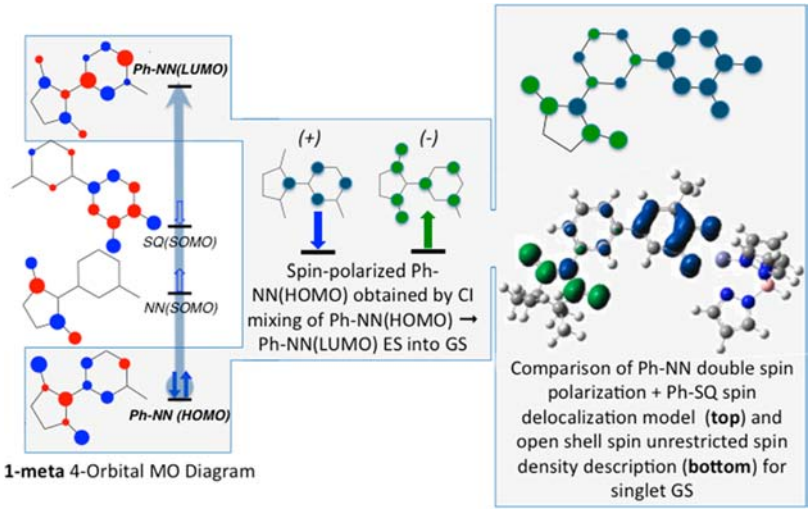


**Figure 8.** (Left and middle) Double spin polarization mechanism in the Ph-NN fragment via the EC1 excited state. (Right) In-phase Ph-NN spin polarization and SQ spin delocalization supporting antiferromagnetic alignment of SQ and NN fragments.

dipoles for the two one-electron contributions to the transition. Band C is markedly more intense in **1-meta** than the corresponding band in **1-para**, and this is most likely due to the presence of a very intense CT band in this spectral region that can be assigned as the SQ(SOMO) → SQ-Ph(e2, LUMO) transition which is primarily localized on the SQ chromophore but possesses SQ → Ph(e2) CT character. In contrast to the SQ → Ph-NN(e1) CT character observed in **1-para**, the phenylene (bridge) orbital of e2 symmetry possesses nodal character at the carbon atoms that attach to the SQ and NN fragments in **1-para** and therefore is essentially nonbonding in character with respect to the SQ and NN frontier orbitals of **1-para** (Figure 6B). Thus, differences in the CT spectra between **1-meta** and **1-para** reveal markedly different interactions between SQ and NN frontier orbitals and the Ph(e1) and Ph(e2) bridge orbitals, and this highlights the effects of connectivity differences between *para*- and *meta*-substituted benzene rings in these biradicals. The dominant SQ(SOMO) → Ph(e2) CT band in **1-meta** is also fully consistent with a marked reduction in the SQ(SOMO) → Ph-NN(e1, LUMO) charge transfer that contributes to the efficient D → A ferromagnetic pathway responsible for strong ferromagnetic coupling in **1-para** (Figure 6B).

**Electronic Origin of the Antiferromagnetic Exchange in 1-meta.** The dominant mechanism for ferromagnetic exchange in **1-para** involves configurational mixing of an SQ(SOMO) → Ph-NN(e1, LUMO) ILCT configuration ($^3$CTC2, Figure 7) into the ground configuration ($^3$GC, Figure 7).[21] In stark contrast to **1-para**, the intensity of the SQ(SOMO) → Ph-NN(e1, LUMO) CT transition for **1-meta** is dramatically reduced. The marked decrease in SQ(SOMO) → Ph-NN(e1, LUMO) CT intensity is a function of the cross-conjugated phenylene bridge connectivity, which has the effect of reducing excited-state ferromagnetic exchange contributions to the ground state and allows antiferromagnetic contributions to dominate. Thus, the observation of ground-state antiferromagnetic exchange coupling in **1-meta** is important and reveals the fact that other orbital pathways are operative. In order to understand the nature of the magnetic exchange pathways in **1-meta** and correlate these pathways with spectroscopic observables, we first construct electronic configurations that result from one-electron promotions to the Ph-NN(HOMO), NN(SOMO), Ph-NN(e1, LUMO), and SQ(SOMO) frontier MOs to form the EC and CTCs of Figure 7. We stress that these orbitals represent a minimum number (i.e., minimal complete active space (CAS)) required to understand how singlet and triplet ECs and CTCs mix into the GS to promote antiferromagnetic exchange coupling of the NN and SQ spins.

Configurational mixing of the EC and CTCs depicted in Figure 7 with the GC stabilizes both the $^1$GS and $^3$GS.[11] Our analysis of the electronic absorption spectrum for **1-meta** provides evidence for the formation of all the singly ECs depicted in Figure 7. We expect that configurational mixing of CTC1 and CTC2 with the GC will result in preferential stabilization of the $^3$GS since the single site (NN) exchange integral ($K_0$) is anticipated to be large ($K_0$ = 2275 cm$^{-1}$ for $Tp^{Cum,Me}Zn(SQ–NN)$).[20] In fact, we have experimentally determined that ~25% of an $^3$CTC2-type configuration is admixed into the $^3$GS of $Tp^{Cum,Me}Zn(SQ–NN)$ resulting in the observation of strong GS ferromagnetic exchange ($J_{SQ–NN} \approx$ +550 cm$^{-1}$). Support for at least some admixture of CTC1 and CTC2 into the $^3$GS of **1-meta** derives from the computed spin density description for the $^3$GS (SI), which shows an increase in spin density on the NN fragment (1.04) compared to the SQ fragment (0.96). Spin population transfer between the SQ and NN fragments[52] derives from the fact that none of the spins in CTC1 and CTC2 are localized on the SQ fragment since the SQ(SOMO) is either doubly occupied or vacant in these triplet configurations and therefore possesses no net spin density.

One way for the $^1$GS to be stabilized with respect to the $^3$GS is by configurational mixing of ECs that lack a triplet counterpart with the $^1$GC to stabilize the $^1$GS. Excited state configurations that lack a triplet counterpart are closed-shell configurations. The closed-shell double excited configurations (DECs) shown in Figure 7 (right) can configurationally mix with the GC in fourth order to selectively stabilize the $^1$GS.[11] The double excited states DEC2 and DEC4 are identical to the states that result from a direct Anderson-type kinetic exchange contribution involving the SQ and NN SOMOs and resemble the metal-to-metal charge transfer (MMCT) states of transition-metal dimers.[11] However, due to the lack of direct orbital overlap between the SQ(SOMO) and the NN(SOMO) the kinetic exchange term is anticipated to be negligible in **1-**


dx.doi.org/10.1021/ja405354x | J. Am. Chem. Soc. 2013, 135, 14713–14725

**meta**. DEC1 and DEC3 are double excitations from the Ph-NN (HOMO) to the two SOMOs and to the Ph-NN (LUMO), respectively. The role of DECs in the stabilization of the $^1$GS is well documented[11,55] and was recently suggested to be important for the stabilization of the $^1$GC in *meta*-poly acene ($n > 3$) bridged Cr(III) dimers.[56]

In spite of the well-known role of DECs contributing to ground-state antiferromagnetic exchange, there is no direct experimental evidence that they contribute to $^1$GS stabilization in **1-meta**. This derives from the fact that band A in singlet **1-meta** and triplet **1-para** are identical, and the VT electronic absorption spectra in the region of band C show that the triplet excited states occur at lower energy than the singlets. The fundamental difference in the electronic absorption spectra of **1-meta** and **1-para** occurs in the region of band B. Here, the SQ(SOMO) → Ph-NN(LUMO) transition that results in ground-state ferromagnetic exchange in **1-para** is dramatically reduced in intensity for **1-meta**. Thus, it would appear that excited-state antiferromagnetism, which contributes to GS antiferromagnetic exchange through CI mixing of DECs with the $^1$GC via $^1$ECs,[11] likely only contributes to a reduction in excited-state ferromagnetic contributions to the GS exchange.

Spin unrestricted broken-symmetry DFT calculations on **1-meta** indicate a large (~0.75 eV) exchange splitting between the spin-up and spin-down orbitals of the Ph-NN(HOMO) orbital resulting from strong exchange interactions between the spin-up and spin-down electrons in the Ph-NN(HOMO) and the unpaired electron spins in the NN(SOMO) and the SQ(SOMO). A spin polarization mechanism[57] can therefore be invoked in order to explain how the $^1$GS is stabilized with respect to the $^3$GS, and we start with a simple spin polarization analysis of occupied Ph-NN(HOMO) orbitals using the four orbital model depicted in Figure 8. Here, configurational mixing of the $^{1,3}$ECs (Figure 7) into the ground state results in a spin polarization of the doubly occupied Ph-NN(HOMO) orbital shown in the center of Figure 8.[52,58,59] The electron−electron repulsion between these spin polarized core electrons and the NN(SOMO) and SQ(SOMO) spins result in a stabilization of the singlet ground configuration ($^1$GC) over the triplet with an antiparallel orientation of the NN(SOMO) and SQ(SOMO) spins. This spin polarization argument also allows one to predict the signs of the atomic spin populations in **1-meta**, and these are in excellent agreement with those computed from a spin-unrestricted DFT calculation of the $^1$GS (Figure 8 right). This analysis underscores the importance of the $^1$EC to the observed magnetic exchange, which arises from a Ph-NN-(HOMO) → Ph-NN(LUMO) one-electron promotion with appreciable contributions from the *m*-Ph bridge.

This analysis can be more quantitatively evaluated in the context of MC-SCF calculations. We initially performed MC-SCF calculations on **1-meta** using an active space spanning just the NN(SOMO) and SQ(SOMO) orbitals. The results of this calculations yield a triplet ground state comprised solely of the $^3$GC depicted in Figure 7 and a small ferromagnetic S-T splitting of $2J = +0.4$ cm$^{-1}$. Increasing the active space to include the Ph-NN(HOMO), SQ(HOMO), NN(SOMO), SQ(SOMO), Ph-NN(e1, LUMO), and Ph(e2, LUMO) orbitals yields a $^1$GS stabilized by $2J = -35$ cm$^{-1}$ (~50% the experimental value) with respect to the $^3$GS, in good agreement with the experimental results ($2J = -64$ cm$^{-1}$). The $^1$GS wave function is found to be dominantly comprised of the $^1$GC (88%) listed in Figure 7 with CI mixing of the $^1$EC (Figure 7; 7%) and a small degree (3%) of an EC resulting from promotion of both Ph-NN(HOMO) electrons to the Ph-NN(e1, LUMO). Interestingly, no closed-shell singlet DECs were observed to contribute to the $^1$GS in the MC-SCF calculations within a cutoff of 1%. The large contribution of the EC (Figure 7) to the ground-state exchange is precisely what we derived from the MO spin polarization analysis detailed above and provides a key state description of the spin density derived from the spin-unrestricted DFT calculations.

**Comparison of Electronic Coupling Through *para*-Phenylene to Electronic Coupling Through *meta*-Phenylene.** One of the fundamental comparisons of electronic coupling between a donor and acceptor is between structures in which the donor and acceptor are connected to a bridge giving rise to a conjugated pathway between donor and acceptor, and structures in which the donor and acceptor are bonded to the bridge such that the $\pi$-pathway from donor to acceptor is cross-conjugated. Indeed, Wasielewski and co-workers[15] as well as Bardeen et al.[23] have shown a factor of ~30 decrease in charge separation rate when a donor and acceptor are bridged by conjugated and cross-conjugated bridges, which in turn suggests an attenuation of $(30)^{1/2} \approx 5.4$ in $\mathbf{H}_{ab}$. However, there has been no report of a direct comparison of $\mathbf{H}_{ab}$ values for the fundamental bridge units, *meta*- and *para*-phenylene. The CI approach to exchange coupling in **1-meta** presented in the previous section allows for such a comparison. One can approximate the relationship between electronic and exchange coupling using eq 5.[10]

$$2J = \frac{\mathbf{H}_{\mathrm{eff}}^2}{\Delta E} \tag{5}$$

If one uses 25 750 cm$^{-1}$ for $\Delta E$ (NN-Ph (HOMO) → NN-Ph (LUMO) energy; Table 1) with $|2J| = 64$ cm$^{-1}$ in eq 5, one can obtain an effective $\mathbf{H}_{ab}$ ($\mathbf{H}_{\mathrm{eff}}$) of 1284 cm$^{-1}$. This value may be compared with an $\mathbf{H}_{\mathrm{eff}} \sim 664$ cm$^{-1}$ obtained by dividing $\mathbf{H}_{ab} = 3632$ cm$^{-1}$ for **1-para**[21] by $(30)^{1/2}$. Thus, eq 5 provides estimation of $\mathbf{H}_{\mathrm{eff}}$ for *m*-Ph which may be compared to the previously determined value of $\mathbf{H}_{ab}$ for **1-para** and is nearly twice the value predicted by the square root of the ratio of charge separation rates in the nonadiabatic regime reported by Wasielewski et al. and Bardeen et al.[23] We note however that distinctly different CI mechanisms contribute to the electronic/exchange coupling in **1-meta** compared to **1-para** such that orbital contributions to $\mathbf{H}_{\mathrm{eff}}$ are quite different from those described by the $\mathbf{H}_{ab}$ value determined for **1-para**. The different CI mechanisms are illustrated schematically in Figure 9: in **1-meta** the electronic/exchange coupling is turned on by the generation of an electron/hole pair involving the Ph-NN

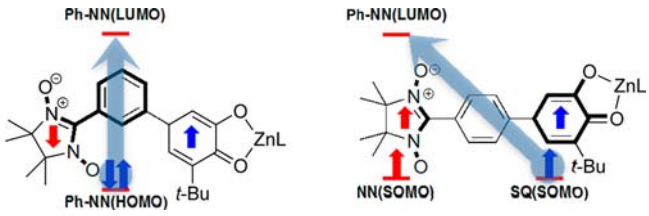


**Figure 9.** Cartoon descriptions of the dominant CI mechanisms for antiferromagnetic exchange coupling of SQ and NN spins in cross-conjugated **1-meta** (left) and ferromagnetic exchange coupling in conjugated **1-para** (right). Note that the exchange interaction in both **1-meta** and **1-para** is zero in the active electron approximation where only the SQ and NN SOMOs are considered.

HOMO and LUMO, while in **1-para**, the electronic/exchange coupling is a consequence of D → A/SQ → Ph-NN(e1, LUMO) charge transfer.

**Relationship to Quantum Interference Effects on the Conductance of Cross-Conjugated Molecules.** The results of this work suggest that configurational mixing of specific ECs into the ground state may be important for modulating electronic communication and electron transport mediated by cross-conjugated bridges. The conductance ($g$) of a molecular junction is related to the transmission probability ($T(E_F)$) evaluated at the Fermi energy according to eq 6.

$$g = \frac{2e^2}{h} T(E_F) \tag{6}$$

The magnitude of the transmission coefficient is proportional to the magnitude of the retarded ($R$) and advanced ($A$) Green's function of the molecule, $\mathbf{G}^{(0)R/A}$, which in turn may be related to frontier MO theory through the Green's function matrix element by eq 7.[60,61]

$$\mathbf{G}_{rl}^{(0)}(E_F) = \sum_k \frac{C_{rk}C_{lk}^*}{E_F - \varepsilon_k \pm i\eta} \tag{7}$$

Here, $r$ and $l$ are the right and left side orbitals of the bridge that are connected to the electrode, $C_{ij}$ are the atomic orbital coefficients of the $k^{th}$ MO located on the left and right atoms of the bridge that spans the electrode, $\varepsilon_k$ is the energy of the $k^{th}$ MO, and $i\eta$ is related to the imaginary part of the Green's function and the local density of states. For cross-conjugated bridge molecules, eq 6 predicts strong antiresonances[16−19,24,25,27,28,62] near the Fermi energy that result in a dramatic reduction in the transmission probability. If we consider the NN and SQ moieties as molecular analogs of biased electrodes and use only the $C_r$ and $C_l$ coefficients for the quaternary carbons of the SQ(SOMO) and NN(SOMO) frontier MOs that connect to the $m$-Ph bridge in **1-meta**, one would expect the transmission at $E_F$ to be zero due to three of the $C_{ij}$ values being equal to zero (Figure 8, left). However, it is important to note that the conductance described by eqs 6 and 7 is a sum over all filled and empty orbitals and not simply the frontier orbitals. The anticipated value of zero for the transmission mediated by the frontier MOs is related to the magnitude of the magnetic exchange interaction ($J \sim 0$) that we calculate for **1-meta** in the active electron approximation,[57] where the active space in the MC-SCF calculations is restricted to the NN(SOMO) and the SQ(SOMO) orbitals. Only through CI mixing of higher energy configurations do we obtain a spin density description of **1-meta** that spans the entire molecule with nonzero spin populations on the carbons that connect to the $m$-Ph bridge and obtain a magnetic exchange interaction that is nonzero. To the extent that CI similarly affects electron transport in cross-conjugated molecule-bridged systems, a state description of electron transport may provide greater insight into important molecular design concepts for control of electron transport in the quantum interference regime.[63−65] In line with our description of the magnetic exchange in **1-meta**, the inclusion of ECs in transport calculations may have the effect of modulating the magnitude of antiresonance contributions to the electron transport by increasing $\pi$-type electronic communication. This idea may also transfer to modulating photoinduced electron-transfer rates in cross-conjugated D−B−A systems as well.[15]

## CONCLUSIONS

We have developed a new synthetic approach to the preparation of catechol−B−NN ligands, which obviates protecting groups used previously.[45] This new approach will allow us to synthesize a diverse array of D−B−A biradical complexes. In addition, we have performed VT-EPR, VT-magnetic susceptibility, and VT-electronic absorption experiments on a new D−B−A biradical (**1-meta**) that possesses a $m$-Ph bridge, and the results show moderate antiferromagnetic exchange coupling between the NN and SQ spin centers. The electronic origin of the magnitude of $2J$ is of extreme interest since **1-meta** is cross-conjugated and, within the active electron approximation, is not anticipated to possess an appreciable exchange interaction due to zero overlap and zero overlap density between the SQ(SOMO) and NN(SOMO). Therefore, in order to understand the mechanism for the observed electronic and magnetic coupling in cross-conjugated **1-meta**, we must move beyond the active electron approximation. Thus, we have evaluated the results of the magnetic and spectroscopic data in the context of detailed bonding, configuration interaction, and spectroscopic computations. Specifically, the spectroscopic results strongly suggest that only one singly excited configuration ($^1$EC) provides a mechanism for antiferromagnetic exchange in **1-meta**. MC-SCF calculations reveal no appreciable configurational mixing of CTCs with the GS, and this is important because a CTC2 configuration resulting from a SQ(SOMO) → Ph-NN(e1, LUMO) one-electron promotion has been shown to be responsible for the observed ferromagnetic exchange in isomeric **1-para** (Figure 7). The minor role of singly excited CTCs to the ground-state exchange coupling in **1-meta** is also supported by the deconvoluted pure singlet and triplet absorption spectra for **1-meta** (Figure 5B). Here, $^3$GS → $^3$ES transitions that contribute to band C in **1-meta** lie ∼500−1000 cm$^{-1}$ lower in energy than the corresponding $^1$GS → $^1$ES transitions. To the extent that these triplet CT excited states configurationally mix with the GS, the energy denominator terms indicate that admixture of excited triplet CTCs with the GC will result in preferential stabilization of the $^3$GS; a result that is opposite of what is observed experimentally (i.e., a singlet GS). Thus, second-order CT contributions to electronic/exchange coupling in cross-conjugated **1-meta** are inherently weak (or negligible) and provide for a unique electronic structure that allows spin polarization contributions to play a dominant role in defining the nature of the ground-state magnetic exchange interaction. From a CI perspective, it appears that smaller $\mathbf{H}_{ab}$ values for cross-conjugated bridges are a natural consequence of inherently weaker CT contributions to the CI expansion of the GS wave function, compared to the stronger CT contributions present in D−B−A systems with conjugated bridges. This concept is in agreement with the results of photoinduced electron-transfer experiments that compare conjugated and cross-conjugated bridges in D−B−A systems.[15]

Our understanding of D−A electronic coupling in **1-meta** may provide new insight into how quantum interference effects[15,16,19,62] on electron transfer/transport can be modulated by excited-state contributions. Thus, by understanding the excited-state origin of the electronic and magnetic exchange coupling in cross-conjugated systems, we have a mechanism by which we can modulate the coupling.

Our conclusions regarding bridge parity effects on D−A electronic coupling directly apply to electron transport in

single-molecule devices since the transmission varies linearly with the square of the electronic coupling matrix element. One important distinction is that in contrast to the growing number of computational and experimental papers describing transmission through conjugated vs cross-conjugated bridges, the "biased electrodes" in D−B−A biradicals are the SQ donor and the NN acceptor, which have $\pi$-contacts to the bridge, whereas the most common single-molecule devices use metal−thiol−bridge−thiol−metal constructs where the $\sigma$-contacts to the bridge appear to dominate. Consequently, the $\sigma$ pathways manifest themselves in the transmission local density of states plots for molecular bridges connected to metallic electrodes by thiol contacts.[15,66] We hypothesize that the transmission in single molecule devices with $\pi$-contacts to the electrodes should be dominated by the bridge/contact $\pi$-system.[67,68] If this is true, it would prove valuable to further explore how bridge substituents might modulate electronic coupling, particularly in the case of cross-conjugated bridges with strong $\pi$-connectivity to donors, acceptors, and nanoelectrode assemblies. Our understanding of the superexchange pathway responsible for electronic coupling in **1-meta** indicates that the addition of electron-withdrawing groups (EWGs) and electron-donating groups (EDGs) oriented *meta* to the D and A, and *para* to A and *ortho* to D will allow for exquisite control of D−A coupling in cross-conjugated systems and provide valuable new insight into quantum interference effects and gated electron transport[69] mediated by cross-conjugated molecules placed between biased electrodes. Efforts along these lines are underway that will determine the effect of EWGs and EDGs on CI contributions to D−A coupling in D−B−A biradicals.

## ■ ASSOCIATED CONTENT

### Supporting Information

X-ray crystallographic details, EPR spectra and DFT-computed spin densities for **1-meta**. This information is available free of charge via the Internet at http://pubs.acs.org.

## ■ AUTHOR INFORMATION


### Corresponding Authors

mkirk@unm.edu
shultz@ncsu.edu

### Present Address

[§]Department of Chemistry, University of Western Ontario, London, Ontario, Canada


### Notes

The authors declare no competing financial interest.

## ■ ACKNOWLEDGMENTS

D.A.S. thanks the National Science Foundation (NSF CHE-1213269) and M.L.K. acknowledges the National Science Foundation (NSF-CHE-1012928) for financial assistance. Funding for the NCSU Department of Chemistry Mass Spectrometry Facility was obtained from the North Carolina Biotechnology Center and the NCSU Department of Chemistry.

## ■ REFERENCES


(1) Aviram, A.; Ratner, M. A. *Chem. Phys. Lett.* **1974**, *29*, 277.
(2) Zeng, Y.; Zimmt, M. B. *J. Phys. Chem.* **1992**, *96*, 8395.
(3) Gosztola, D.; Wang, B.; Wasielewski, M. R. *J. Photochem. Photobiol., A* **1996**, *102*, 71.
(4) Lukas, A. S.; Bushard, P. J.; Weiss, E. A.; Wasielewski, M. R. *J. Am. Chem. Soc.* **2003**, *125*, 3921.
(5) Weiss, E. A.; Ahrens, M. J.; Sinks, L. E.; Gusev, A. V.; Ratner, M. A.; Wasielewski, M. R. *J. Am. Chem. Soc.* **2004**, *126*, 5577.
(6) Sinks, L. E.; Weiss, E. A.; Giaimo, J. M.; Wasielewski, M. R. *Chem. Phys. Lett.* **2005**, *404*, 244.
(7) Weiss, E. A.; Tauber, M. J.; Kelley, R. F.; Ahrens, M. J.; Ratner, M. A.; Wasielewski, M. R. *J. Am. Chem. Soc.* **2005**, *127*, 11842.
(8) Weiss, E. A.; Wasielewski, M. R.; Ratner, M. A. *J. Chem. Phys.* **2005**, *123*, 064504.
(9) Okamura, M. Y., Fredkin, D. R.; Isaacson, R. A.; Feher, G. In *Tunnelling in Biological Systems, Johnson Research Foundation Symposium*; Chance, B. , Ed.; Academic Press: New York, 1978; p 729.
(10) Anderson, P. W. *Phys. Rev.* **1959**, *115*, 2.
(11) Tuczek, F.; Solomon, E. I. *J. Am. Chem. Soc.* **1994**, *116*, 6916.
(12) Tuczek, F.; Solomon, E. I. *Inorg. Chem.* **1993**, *32*, 2850.
(13) Weiss, E. A.; Tauber, M. J.; Ratner, M. A.; Wasielewski, M. R. *J. Am. Chem. Soc.* **2005**, *127*, 6052.
(14) Davis, W. B.; Svec, W. A.; Ratner, M. A.; Wasielewski, M. R. *Nature* **1998**, *396*, 60.
(15) Ricks, A. B.; Solomon, G. C.; Colvin, M. T.; Scott, A. M.; Chen, K.; Ratner, M. A.; Wasielewski, M. R. *J. Am. Chem. Soc.* **2010**, *132*, 15427.
(16) Andrews, D. Q.; Solomon, G. C.; Van Duyne, R. P.; Ratner, M. A. *J. Am. Chem. Soc.* **2008**, *130*, 17309.
(17) Solomon, G. C.; Andrews, D. Q.; Goldsmith, R. H.; Hansen, T.; Wasielewski, M. R.; Van Duyne, R. P.; Ratner, M. A. *J. Am. Chem. Soc.* **2008**, *130*, 17301.
(18) Solomon, G. C.; Andrews, D. Q.; Van Duyne, R. P.; Ratner, M. A. *J. Am. Chem. Soc.* **2008**, *130*, 7788.
(19) Hansen, T.; Solomon, G. C.; Andrews, D. Q.; Ratner, M. A. *J. Chem. Phys.* **2009**, *131*, 194704.
(20) Kirk, M. L.; Shultz, D. A.; Depperman, E. C.; Brannen, C. L. *J. Am. Chem. Soc.* **2007**, *129*, 1937.
(21) Kirk, M. L.; Shultz, D. A.; Depperman, E. C.; Habel-Rodriguez, D.; Schmidt, R. D. *J. Am. Chem. Soc.* **2012**, *134*, 7812.
(22) Kirk, M. L.; Shultz, D. A. *Coord. Chem. Rev.* **2013**, *257*, 218.
(23) Thompson, A. L.; Ahn, T. S.; Thomas, K. R. J.; Thayumanavan, S.; Martinez, T. J.; Bardeen, C. J. *J. Am. Chem. Soc.* **2005**, *127*, 16348.
(24) Arroyo, C. R.; Tarkuc, S.; Frisenda, R.; Seldenthuis, J. S.; Woerde, C. H. M.; Eelkema, R.; Grozema, F. C.; van der Zant, H. S. J. *Angew. Chem., Int. Ed.* **2013**, *52*, 3152.
(25) Baer, R.; Neuhauser, D. *J. Am. Chem. Soc.* **2002**, *124*, 4200.
(26) Vazquez, H.; Skouta, R.; Schneebeli, S.; Kamenetska, M.; Breslow, R.; Venkataraman, L.; Hybertsen, M. S. *Nat. Nanotechnol.* **2012**, *7*, 663.
(27) Patoux, C.; Coudret, C.; Launay, J. P.; Joachim, C.; Gourdon, A. *Inorg. Chem.* **1997**, *36*, 5037.
(28) Solomon, G. C.; Andrews, D. Q.; Hansen, T.; Goldsmith, R. H.; Wasielewski, M. R.; Van Duyne, R. P.; Ratner, M. A. *J. Chem. Phys.* **2008**, *129*, 054701.
(29) Paulson, B. P.; Curtiss, L. A.; Bal, B.; Closs, G. L.; Miller, J. R. *J. Am. Chem. Soc.* **1996**, *118*, 378.
(30) Shephard, M. J.; Paddonrow, M. N.; Jordan, K. D. *J. Am. Chem. Soc.* **1994**, *116*, 5328.
(31) Liang, C. X.; Newton, M. D. *J. Phys. Chem.* **1992**, *96*, 2855.
(32) Onuchic, J. N.; Beratan, D. N. *J. Am. Chem. Soc.* **1987**, *109*, 6771.
(33) Beratan, D. N.; Hopfield, J. J. *J. Am. Chem. Soc.* **1984**, *106*, 1584.
(34) Skourtis, S. S.; Waldeck, D. H.; Beratan, D. N. *J. Phys. Chem. B* **2004**, *108*, 15511.
(35) Kirk, M. L.; Shultz, D. A.; Depperman, E. C. *Polyhedron* **2005**, *24*, 2880.
(36) Tuczek, F.; Solomon, E. I. *Coord. Chem. Rev.* **2001**, *219*, 1075.
(37) Chen, C. T.; Kao, J. Q.; Salunke, S. B.; Lin, Y. H. *Org. Lett.* **2011**, *13*, 26.
(38) Holbach, M.; Weck, M. *J. Org. Chem.* **2006**, *71*, 1825.
(39) Magdziak, D.; Rodriguez, A. A.; Van De Water, R. W.; Pettus, T. R. R. *Org. Lett.* **2002**, *4*, 285.

(40) Shimono, S.; Tamura, R.; Ikuma, N.; Takimoto, T.; Kawame, N.; Tamada, O.; Sakai, N.; Matsuura, H.; Yamauchi, J. *J. Org. Chem.* **2004**, *69*, 475.
(41) Ruf, M.; Vahrenkamp, H. *Inorg. Chem.* **1996**, *35*, 6571.
(42) Frisch, M. J.; G. W. T., Schlegel, H. B.; Scuseria, G. E.; Robb, M. A.; Cheeseman, J. R.; Montgomery, J. A., Jr.; Vreven, T.; Kudin, K. N.; Burant, J. C.; Millam, J. M.; Iyengar, S. S.; Tomasi, J.; Barone, V.; Mennucci, B.; Cossi, M.; Scalmani, G.; Rega, N.; Petersson, G. A.; Nakatsuji, H.; Hada, M.; Ehara, M.; Toyota, K.; Fukuda, R.; Hasegawa, J.; Ishida, M.; Nakajima, T.; Honda, Y.; Kitao, O.; Nakai, H.; Klene, M.; Li, X.; Knox, J. E.; Hratchian, H. P.; Cross, J. B.; Bakken, V.; Adamo, C.; Jaramillo, J.; Gomperts, R.; Stratmann, R. E.; Yazyev, O.; Austin, A. J.; Cammi, R.; Pomelli, C.; Ochterski, J. W.; Ayala, P. Y.; Morokuma, K.; Voth, G. A.; Salvador, P.; Dannenberg, J. J.; Zakrzewski, V. G.; Dapprich, S.; Daniels, A. D.; Strain, M. C.; Farkas, O.; Malick, D. K.; Rabuck, A. D.; Raghavachari, K.; Foresman, J. B.; Ortiz, J. V.; Cui, Q.; Baboul, A. G.; Clifford, S.; Cioslowski, J.; Stefanov, B. B.; Liu, G.; Liashenko, A.; Piskorz, P.; Komaromi, I.; Martin, R. L.; Fox, D. J.; Keith, T.; M. A. Al-Laham, Peng, C. Y.; Nanayakkara, A.; Challacombe, M.; Gill, P. M. W.; Johnson, B.; Chen, W.; Wong, M. W.; Gonzalez, C.; Pople, J. A. *Gaussian 09*; Gaussian, Inc.: Wallingford, CT, 2004.
(43) Electron density difference maps (EDDMs) were constructed utilizing the "EDDM, Transition Density, and Orbital Generation for ADF and Gaussian 03" program written by Mr. Benjamin Stein at the UNM Department of Chemistry and Chemical Biology, 2011.
(44) Neese, F.; Wennmohs, F.; Becker, U.; Ganyushin, D.; Hansen, A.; Liakos, D. G.; Kollmar, C.; Kossmann, S.; Petrenko, T.; Reimann, C.; Riplinger, C.; Sivalingam, K.; Valeev, E.; Wezisla, B. *ORCA - An ab initio, DFT and semiempirical SCF-MO package*; 2.8-00 ed., 2009
(45) Shultz, D. A.; Vostrikova, K. E.; Bodnar, S. H.; Koo, H. J.; Whangbo, M. H.; Kirk, M. L.; Depperman, E. C.; Kampf, J. W. *J. Am. Chem. Soc.* **2003**, *125*, 1607.
(46) Shultz, D. A.; Bodnar, S. H.; Vostrikova, K. E.; Kampf, J. W. *Inorg. Chem.* **2000**, *39*, 6091.
(47) Ruf, M.; Noll, B. C.; Groner, M. D.; Yee, G. T.; Pierpont, C. G. *Inorg. Chem.* **1997**, *36*, 4860.
(48) Shultz, D. A.; Bodnar, S. H. *Inorg. Chem.* **1999**, *38*, 591.
(49) *Magnetic Properties of Organic Materials*; Lahti, P. M., Ed.; Marcel Dekker: New York, 1999.
(50) Lanfranc de Panthou, F.; Luneau, K.; Musin, R.; Öhrström, L.; Grand, A.; Turek, P.; Rey, P. *Inorg. Chem.* **1996**, *35*, 3484.
(51) Lanfranc de Panthou, F.; Luneau, D.; Laugier, J.; Rey, P. *J. Am. Chem. Soc.* **1993**, *115*, 9095.
(52) Kirk, M. L.; Shultz, D. A.; Habel-Rodriguez, D.; Schmidt, R. D.; Sullivan, U. *J. Phys. Chem. B* **2010**, *114*, 14712.
(53) Putz, A. M.; Schatzschneider, U.; Rentschler, E. *Phys. Chem. Chem. Phys.* **2012**, *14*, 1649.
(54) Carrington, A.; McLachlan, A. D. *Introduction to Magnetic Resonance*; Chapman and Hall: New York, 1979.
(55) Barnes, A. D. J.; Baikie, T.; Hardy, V.; Lepetit, M.-B.; Maignan, A.; Young, N. A.; Francesconi, M. G. *J. Mater. Chem.* **2006**, *16*, 3489.
(56) Nunzi, F.; Ruiz, E.; Cano, J.; Alvarez, S. *J. Phys. Chem. C* **2007**, *111*, 618.
(57) Kahn, O. *Molecular Magnetism*; VCH: New York, 1993.
(58) Zheludev, A.; Barone, V.; Bonnet, M.; Delley, B.; Grand, A.; Ressouche, E.; Rey, P.; Subra, R.; Schweizer, J. *J. Am. Chem. Soc.* **1994**, *116*, 2019.
(59) Cirujeda, J.; Vidal-Gancedo, J.; Jürgens, O.; Mota, F.; Novoa, J. J.; Rovira, C.; Veciana, J. *J. Am. Chem. Soc.* **2000**, *122*, 11393.
(60) Tsuji, Y.; Staykov, A.; Yoshizawa, K. *J. Am. Chem. Soc.* **2011**, *133*, 5955.
(61) Priyadarshy, S.; Skourtis, S. S.; Risser, S. M.; Beratan, D. N. *J. Chem. Phys.* **1996**, *104*, 9473.
(62) Bihary, Z.; Ratner, M. A. *Adv. Quantum Chem.* **2005**, *48*, 23.
(63) Yeganeh, S.; Ratner, M. A.; Galperin, M.; Nitzan, A. *Nano Lett.* **2009**, *9*, 1770.
(64) Delaney, P.; Greer, J. C. *Int. J. Quantum Chem.* **2004**, *100*, 1163.
(65) Delaney, P.; Greer, J. C. *Phys. Rev. Lett.* **2004**, *93*, 036805.
(66) Ke, S. H.; Yang, W. T.; Baranger, H. U. *Nano Lett.* **2008**, *8*, 3257.
(67) Meisner, J. S.; Ahn, S.; Aradhya, S. V.; Krikorian, M.; Parameswaran, R.; Steigerwald, M.; Venkataraman, L.; Nuckolls, C. *J. Am. Chem. Soc.* **2012**, *134*, 20440.
(68) Hipps, K. W. *Science* **2001**, *294*, 536.
(69) Cardamone, D. M.; Stafford, C. A.; Mazumdar, S. *Nano Lett.* **2006**, *6*, 2422.